Procedia Manufacturing

Volume 5, 2016, Pages 248–258

44th Proceedings of the North American Manufacturing Research Institution of SME http://www.sme.org/namrc

Modelling of Fracture Onset in Ti6Al4V Sheets Deformed at Elevated Temperature

Beatrice Valoppi[1*], Stefania Bruschi[1] and Andrea Ghiotti[1]

[1]*University of Padova, Padova, Italy.*

beatrice.valoppi@dii.unipd.it, stefania.bruschi@unipd.it, andrea.ghiotti@unipd.it

Abstract

The reliability of FE-based simulations, employed to assess the application of sheet forming process at elevated temperature to the production of high surface-to-thickness ratio components, depends on the accuracy of the models used to describe the material behavior. In this paper, a modified version of the uncoupled Johnson-Cook fracture criterion is proposed to predict the fracture onset when deforming Ti6Al4V sheets of 1 mm thickness in a wide range of temperature spanning from room temperature to 900°C. Tensile tests were performed at different temperatures and strain rates on smooth and notched samples, leading to different values of the stress triaxiality factor. The resulting strains at fracture were used to both calibrate and validate the modified fracture criterion in two temperature ranges, namely 25-600°C and 600-900°C.

Keywords: Ductile fracture, Elevated temperature, Sheet forming, Ti6Al4V

1 Introduction

The use of the Ti6Al4V titanium alloy spreads out in the military and aerospace industries, as well as in the biomedical sector thanks to its high strength-to-weight ratio, elevated corrosion resistance and biocompatibility (Li, et al., 2014; Odenberger, et al., 2013; Majorell, et al., 2002; Lin, et al., 2014). Plastic deformation processes, machining operations, and, more recently, novel additive manufacturing technologies are widely employed to produce parts made of Ti6Al4V. In case of components characterized by a high surface-to-thickness ratio, sheet forming processes are usually carried out, but the Ti6Al4V limited formability at room temperature forces their conduction at elevated temperature, which allows also reducing springback and, therefore, increasing the part geometrical accuracy (Chen & Chiu , 2005).

The choice of the proper parameters to conduct these forming processes passes through an overall investigation of the material behaviour under a wide range of testing conditions, i.e. temperature and

* Beatrice Valoppi,
Via Venezia 1, 35131 Padova, Italy

 Selection and peer-review under responsibility of the Scientific Programme Committee of NAMRI/SME

doi:10.1016/j.promfg.2016.08.022

strain rate, but also through the development of FE-based models able to accurately predict the process outcomes and therefore to help in its design and optimization. However, the reliability of the simulation results strongly depends on the accuracy of the models used to describe the material rheology and fracture occurrence, the latter particularly sensitive in case of sheet forming processes (Tan, et al., 2015; Guzmán, et al., 2015). The failure in sheet forming operations is commonly predicted using the method of the Forming Limit Diagrams (FLD), used both at academic level and in the industrial practise (Merklein, et al., 2015). However, because each FLD depends on the sheet thickness, temperature and strain rate, the prediction of failure in a wide range of process conditions, which are typical of sheet forming processes carried out at elevated temperature, required great experimental efforts when using this method. Therefore, the necessity to overcome this disadvantage pushed the research to apply alternative methods, based on fracture criteria (Bruschi, et al., 2014), using either coupled or uncoupled approaches (Li, et al., 2011). The coupled criteria take into consideration the effect of the progressive material damage on the material flow stress, whereas when applying uncoupled approaches the yield surface sensitivity to the damage evolution is neglected. However, even if the coupled fracture criteria are based on the physical mechanism of the damage evolution and are considered to better describe the phenomena underlying the fracture occurrence, they are barely applied in industrial applications due to their complexity and difficulty in calibration (Ling-Yun, et al., 2015). On the other hand, the uncoupled approaches have been widely used since they have a simple formulation and require an easy calibration (Li, et al., 2011).

The aim of the paper is therefore to present a modified version of an uncoupled fracture mechanics-based criterion, which can accurately predict the fracture occurrence in metal sheets deformed under a wide range of temperatures at different strain rates, considering also the influence of the stress state in the material being deformed. In particular, a modified version of the Johnson-Cook criterion (Gordon & Johnson, 1985) is proposed in the paper to predict the fracture onset in Ti6Al4V sheets deformed in a range of temperatures spanning from room temperature to 900°C. The modified criterion was calibrated and validated using complementary experimental and numerical techniques. Tensile tests on smooth and notched samples were carried out to evaluate the material strain at fracture sensitivity to the temperature, strain rate, and stress triaxiality. The numerical models of the tensile tests conducted on the notched samples were developed to determine the average values of the stress triaxiality factor, and, therefore, correlate them to the strain at fracture values. Finally, the validation of the proposed criterion was carried out on testing cases different from those utilized for its calibration, proving its predictive capability in a wide range of testing conditions.

2 Background

The Johnson-Cook fracture criterion describes the strain at fracture as a function of the stress triaxiality factor, the strain rate and the temperature, as reported in Eq. (1) (Gordon & Johnson, 1985).

$$\varepsilon_F = \left[D_1 + D_2 \cdot e^{D_3 \cdot \sigma^*}\right][1 + D_4 \cdot \ln \dot{\varepsilon}^*][D_5 \cdot T^* + 1] \quad (1)$$

The first term into brackets describes the influence of the stress triaxiality factor, σ^*, which has to be lower than 1.5 (Gordon & Johnson, 1985). The stress triaxiality factor is a dimensionless pressure defined as:

$$\sigma^* = \frac{-p}{\bar{\sigma}} = \frac{\sigma_m}{\bar{\sigma}} \quad (2)$$

where σ_m is the hydrostatic pressure and $\bar{\sigma}$ the Von Mises equivalent stress. Through these two parameters, the stress triaxiality factor is related to both the hydrostatic and deviatoric stress tensors in which a general stress tensor, σ, can be divided. The hydrostatic stress tensor is represented by the hydrostatic pressure, which can be expressed as

$$p = -\sigma_m = -\frac{1}{3}(\sigma_1 + \sigma_2 + \sigma_3) \quad (3)$$

where σ_i are the principal stresses of the general stress tensor σ (Algarni, et al., 2015). The deviatoric stress tensor, in terms of its second invariant J_2, is represented through the Von Mises equivalent stress (Ling-Yun, et al., 2015), which can be expressed through the following equation:

$$\bar{\sigma} = \sqrt{3J_2} = \frac{1}{\sqrt{2}}\sqrt{(\sigma_1 - \sigma_2)^2 + (\sigma_2 - \sigma_3)^2 + (\sigma_3 - \sigma_1)^2} \quad (4)$$

The effect of the strain rate is described using the dimensionless strain rate parameter, $\dot{\varepsilon}^*$, which is defined as the ratio between the strain rate, $\dot{\varepsilon}$, and the reference strain rate, $\dot{\varepsilon}_{ref}$. According to (Gordon & Johnson, 1985) and (He, et al., 2013) $\dot{\varepsilon}^*$ can be expressed as reported in the following equation

$$\dot{\varepsilon}^* = \frac{\dot{\varepsilon}}{\dot{\varepsilon}_{ref}} \quad (5)$$

The last factor, representing the effect of the temperature, is a function of the homologous temperature, T^*, which can be defined as

$$T^* = \frac{T - T_{ref}}{T_m - T_{ref}} \quad (6)$$

based on (Gordon & Johnson, 1985) and (He, et al., 2013). In this equation, T is the testing temperature, T_{ref} the reference testing temperature, and T_m the material melting temperature. According to (Boyer, et al., 1994), the Ti6Al4V melting temperature was assumed to be 1650°C.

3 Experiments and simulations

The tested material was the Ti6Al4V titanium alloy, purchased from Titanium Consulting & Trading™ in form of 1 mm thick sheets in the annealed condition. The material chemical composition and main properties provided by the supplier are reported in Table 1, while the different shapes of the samples cut from the sheets are shown in Figure 1a. Two different sets of tensile tests were carried out a 5 t universal MTS™ testing machine (Figure 1b), one on smooth samples to evaluate the strain at fracture sensitivity to the temperature and strain rate, and one on notched samples to evaluate the strain at fracture sensitivity to the stress triaxiality, but at fixed temperature and strain rate. Afterwards, the tensile tests on the notched samples were numerically simulated to evaluate the values of the stress triaxiality factor and correlate them to the strain at fracture, which is mandatory for the identification of the material constants of the proposed fracture criterion.

Chemical composition [wt%]					UTS [MPa]	Y [MPa]
Al	Fe (max)	O (max)	Ti	V	950	880
6	0.2	0.2	90	4		

Table 1: Chemical and mechanical properties of the Ti6Al4V alloy.

3.1 Tensile tests on smooth samples

Table 2 reports the experimental plan of the tensile tests on smooth samples (S). A frontal inductor was used to heat the sample central area up to the testing temperature while the temperature was read by the k-type thermocouple spot-welded on the sample central zone (Figure 1c). Once the target temperature was reached, a soaking time of 30 s at this temperature allowed the homogenization of both the temperature and microstructure. At the end of the soaking time, the sample was stretched to failure, maintaining the temperature of the gauge length constant. Before testing, the samples were sprayed with a pattern of random points to let the Aramis™ system from GOM™ calculate the evolution of the true strain thanks to the in-line acquisition of the points displacements through a Charged-Coupled Device (CCD) camera (Figure 1c). To calculate the true stress-true strain curves, the specimen gauge length was fixed at 65 mm for the room-temperature tests and at 15 mm for the tests at higher temperatures, the latter identified on the basis of the recordings of an infra-red thermo-camera. The strain at fracture

was calculated on the basis of the fracture area, which was measured through Scanning Electron Microscopy (SEM) observations.

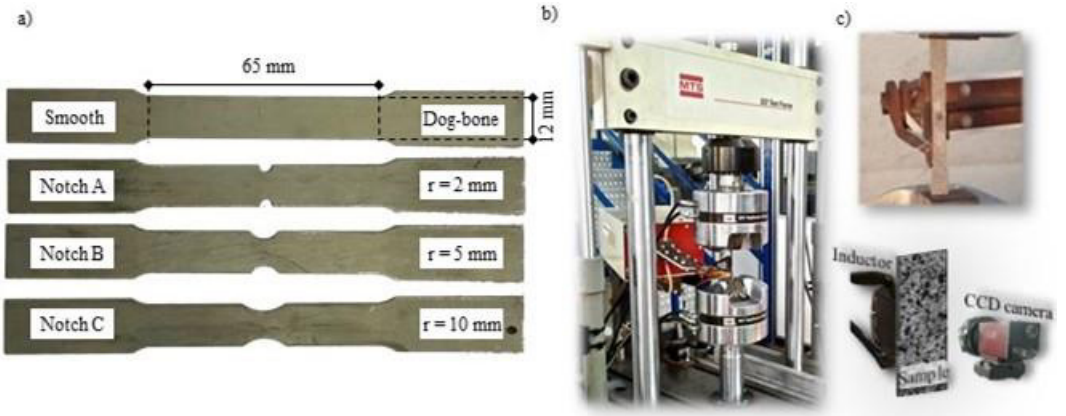

Figure 1. a) Shapes and dimensions of the specimens used for the tensile tests. b) MTS™ tensile testing machine. c) Images of the heating system, sheet sample with the sprayed pattern, and Aramis™ system.

Temperature [°C]							Strain rate [s^{-1}]	Strain
25	200	400	600	700	800	900	0.1	ε_F
25	200	400	600	700	800	900	1	ε_F

Table 2: Experimental plan for the tensile tests on smooth samples.

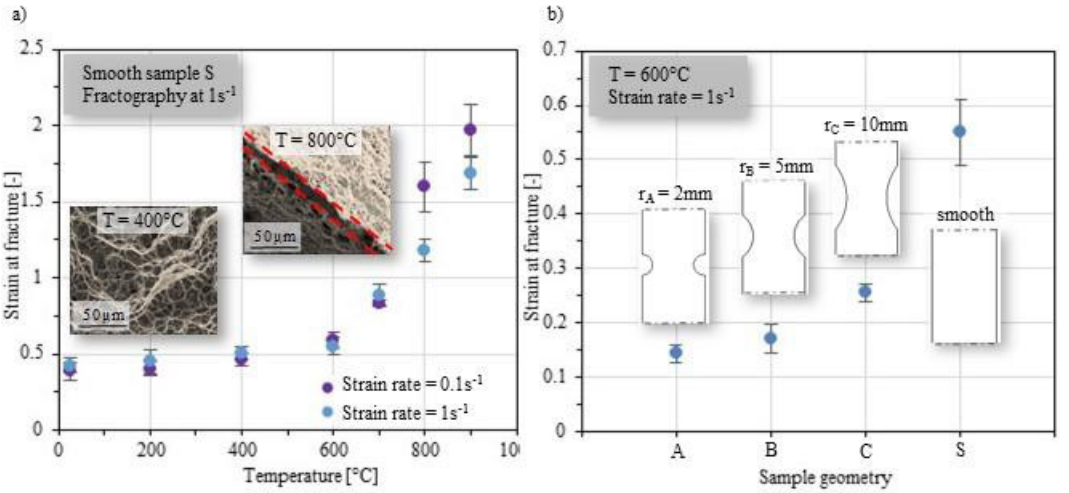

Figure 2: a) Strain at fracture sensitivity to temperature and strain rate for smooth samples and fracture surfaces at 1 s^{-1} and different temperatures. b) Sample drawing details and strain at fracture sensitivity to sample geometry.

Figure 2a shows the influence of the temperature and strain rate on the strain at fracture for the smooth samples: the strain at fracture increases rapidly above 600°C, whereas the temperature influence is less significant below 600°C. The same tendency can be observed for both the strain rates, but the effect of the strain rate on the strain at fracture becomes more significant above 800°C. The increase of ductility in the high temperature range is proved also by the analysis of the fracture surfaces, which shows a significant increase of the necking effect passing from 400°C to 800°C (Valoppi, et al., 2014).

While the same magnification allows observing the details of the fracture surface at 400°C with its characteristic dimples, at 800°C the fracture surface is so sharp that it results to be a very thin row, which is enlightened with two dotted lines in Figure 2a.

3.2 Tensile tests on notched samples

On the basis of the strain at fracture sensitivity to the temperature, the reference testing temperature was assumed to be 600°C since it is the temperature at which the material ductility starts increasing (Figure 2a), while the reference strain rate was set equal to 1 s^{-1}. Accordingly, the tensile tests were carried out at 600°C and 1 s^{-1} on notched samples characterized by three different notch radii (named A, B and C in Figure 1a and in Figure 2b) leading to different values of the stress triaxiality (Ling-Yun, et al., 2015). As for the smooth samples, the strains at fracture were measured and the resulting values are reported in Figure 2b as a function of the sample geometry.

3.3 Numerical modeling of the tensile tests

The numerical models of the tensile tests carried out on the smooth and notched samples were developed using the software Forge© by Transvalor. The material flow stress behaviour was described using the Hansel-Spittel law with five material constants (Eq. (7)), which were identified on the basis of flow stress data obtained from the tensile tests on the smooth samples. The Hansel-Spittel (H-S) model was identified for the two temperature ranges, namely Range A (25-600°C) and Range B (600-900°C), which correspond to the different material behaviour in terms of ductility as shown in Figure 2a. The material constants in these temperature ranges are reported in Table 3 and Table 4, respectively. Figure 3a shows the comparison between the experimental and predicted flow stress curves at 1 s^{-1} and different temperatures.

$$\sigma = Ae^{Tm_1}\varepsilon^{m_2}e^{\frac{m_4}{\varepsilon}}\dot{\varepsilon}^{m_3} \tag{7}$$

A	m_1	m_2	m_3	m_4
1564	-0.001	0.044	0.008	-0.008

Table 3: Hansel-Spittel material constants for temperature Range A (25-600°C).

A	m_1	m_2	m_3	m_4
10012	-0.004	0.002	0.034	-0.007

Table 4: Hansel-Spittel material constants for temperature Range B (600-900°C).

The thermal field of the samples surface, as recorded at the end of the soaking time by means of an infrared thermo-camera, was accurately reproduced (Figure 3b) as well as the samples geometries and applied testing parameters. The mesh size in the zone of the notches was progressively refined until a further decrease did not lead to a significant variation in the simulation results, but only to a relevant increase in the computation time. As it can be seen in Figure 4a, the load-displacement curves recorded from the central point of the notched sample C are barely influenced by the two applied mesh sizes.

Figure 4b reports the stress triaxiality factor as a function of the strain for both the smooth and notched samples from the results of the numerical simulations. The values of the stress triaxiality were recorded in the neck zone of the samples by means of local Lagrangian sensors (see Figure 4a). It is worth to note that the variation of the stress triaxiality with the strain is negligible for all the notched samples (Børvik, et al., 2001) with the expected increase at decreasing the sample notch (Gordon & Johnson, 1985), whereas a slight dependency on the strain can be noticed for the smooth sample, in agreement with (Børvik, et al., 2001). Based on these numerical results, Table 5 reports the values of the stress triaxiality factor for the smooth and notched samples in the reference conditions.

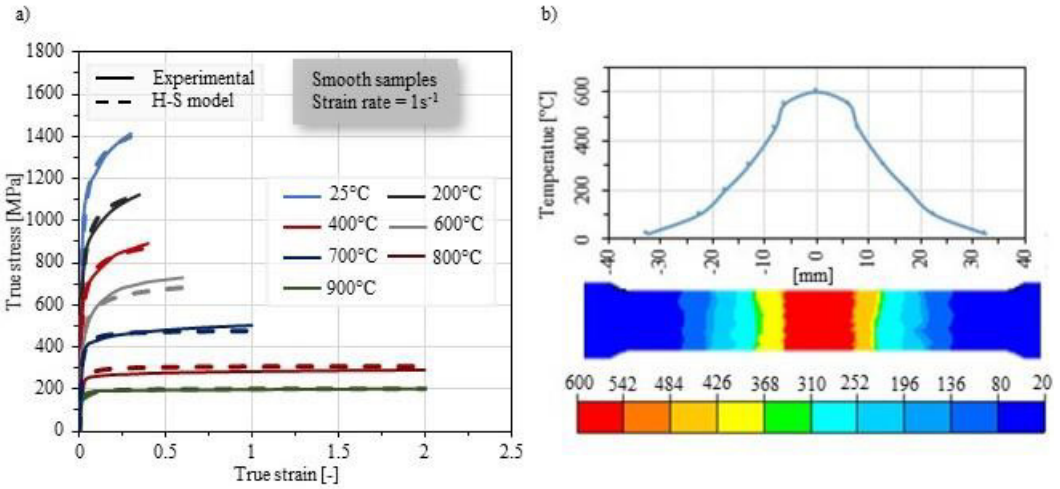

Figure 3: a) Comparison between the experimental and predicted flow stress curves at 1 s^{-1}. b) Example of the sample thermal field imposed in the FE model.

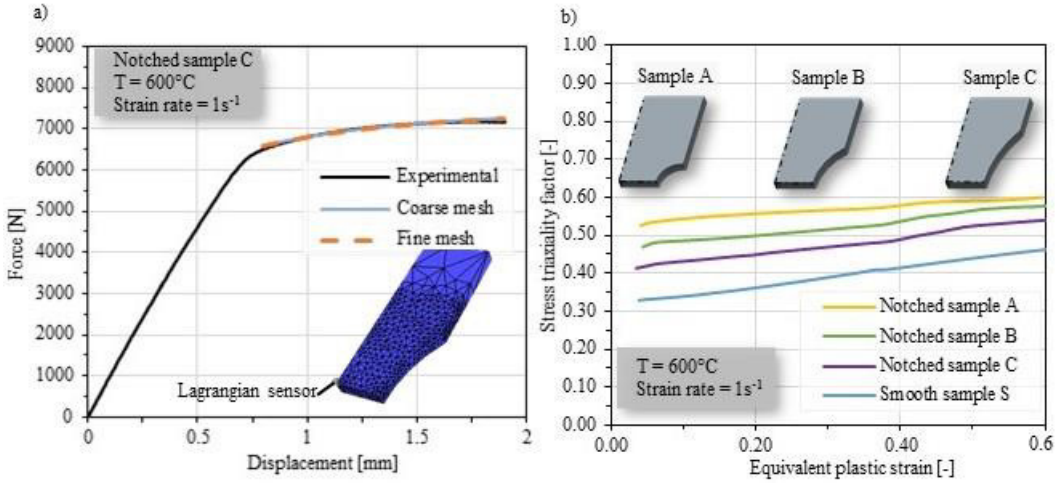

Figure 4: a) Effect of the mesh size on the load-displacement curves. b) Stress triaxiality factor dependence on the strain for the smooth and notched samples.

Sample Geometry	Stress triaxiality factor [-]
Sample A	0.55
Sample B	0.49
Sample C	0.46
Sample S	0.43

Table 5: Values of the stress triaxiality factor for the different sample geometries in the reference conditions.

4 Fracture onset modelling

The results of the tensile tests and numerical simulations are employed to identify the material constants of the modified Johnson-Cook fracture criterion. While the strain at fracture sensitivities to the stress triaxiality factor and strain rate assessed in the original Johnson-Cook criterion are considered valid, the effect of the temperature was modified according to the ductility characteristics of the material (Figure 2a). In the following, the procedure for the material constants identification, the description of the modifications as well as the criterion validation, are fully described.

4.1 Modification and calibration of the Johnson-Cook fracture criterion

The material constants of Eq. (1) are identified through different steps, which start with the analysis of the sole stress triaxiality effect and go on with the strain at fracture sensitivity to the strain rate and temperature, respectively (Børvik, et al., 2001; Gordon & Johnson, 1985).

At the reference conditions, Eq. (1) becomes Eq. (8), which allows the identification of the material constants related to the stress triaxiality factor, namely D_1, D_2 and D_3:

$$\varepsilon_F = \left[D_1 + D_2 \cdot e^{D_3 \cdot \sigma^*}\right] \tag{8}$$

The material constants listed in the Table reported in Figure 5a were identified through a non-linear regression analysis from the data reported in Table 5; Figure 5a shows also the comparison between the experimental and predicted values of the strain at fracture as a function of the stress triaxiality factor proving a satisfactory agreement, which is also witnessed by the value of the correlation coefficient R^2.

The constant D_4, defining the strain at fracture sensitivity to the strain rate in Eq. (1), is identified considering the experimental results of the tensile tests performed at the reference temperature of 600°C but different strain rates (Figure 2a). At these testing conditions, Eq. (1) reduces to:

$$\frac{\varepsilon_F}{\left[D_1 + D_2 \cdot e^{D_3 \cdot \sigma^*}\right]} = \left[1 + D_4 \cdot \ln \dot{\varepsilon}^*\right] \tag{9}$$

Therefore, the curve $\frac{\varepsilon_f}{\left[D_1 + D_2 \cdot e^{D_3 \cdot \sigma^*}\right]}$ vs $\ln \dot{\varepsilon}^*$ can be plotted with the material constant D_4 representing the slope of the linear fitting. Its value and the comparison between the experimental results and predicted data, calculated using Eq. (9) and the constants values from Eq. (8), are shown in Figure 5b, showing again a good fitting.

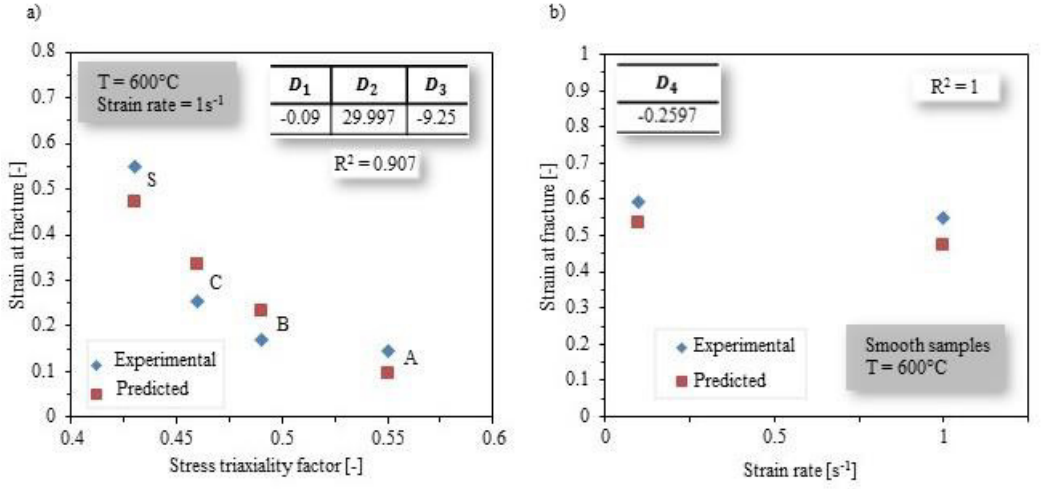

Figure 5: Comparison between the experimental and predicted strains at fracture as a function of a) the stress triaxiality factor, and b) of the strain rate at the reference temperature.

The last parameter to consider in Eq. (1) is the temperature. At the reference strain rate, Eq. (1) can be expressed as follows:

$$\frac{\varepsilon_F}{[D_1+D_2\cdot e^{D_3\cdot\sigma^*}]} = [D_5 \cdot T^* + 1] \tag{10}$$

The value of D_5 can be calculated using the experimental data resulting from the tensile tests performed at the reference strain rate and different temperatures. Since the strain at fracture evolution as a function of the temperature is not constant (Figure 2a), the two ranges of temperatures, namely Range A and Range B, were separately considered in the procedure for the identification of the material constant D_5.

Within Range A, where the relationship between the strain at fracture-to-triaxiality factor ratio and the homologous temperature can be considered linear, as shown in Figure 6a, Eq. (10) is assessed valid. According to this, D_5 is identified as the slope of the linear curve $\frac{\varepsilon_f}{[D_1+D_2\cdot e^{D_3\cdot\sigma^*}]}$ vs T^*. However, to increase the match between the experimental and predicted values, another constant was added to Eq. (10) that becomes Eq. (11). The resulting value of D_5 and D_6, as well as the comparison between the experimental data and calculated strains at fracture, are highlighted in Figure 6b. It can be said that the introduced modification allows predicting the experimental results with a good accuracy, since the correlation coefficient is equal to 0.992.

$$\frac{\varepsilon_F}{[D_1+D_2\cdot e^{D_3\cdot\sigma^*}]} = [D_5 \cdot T^* + D_6] \tag{11}$$

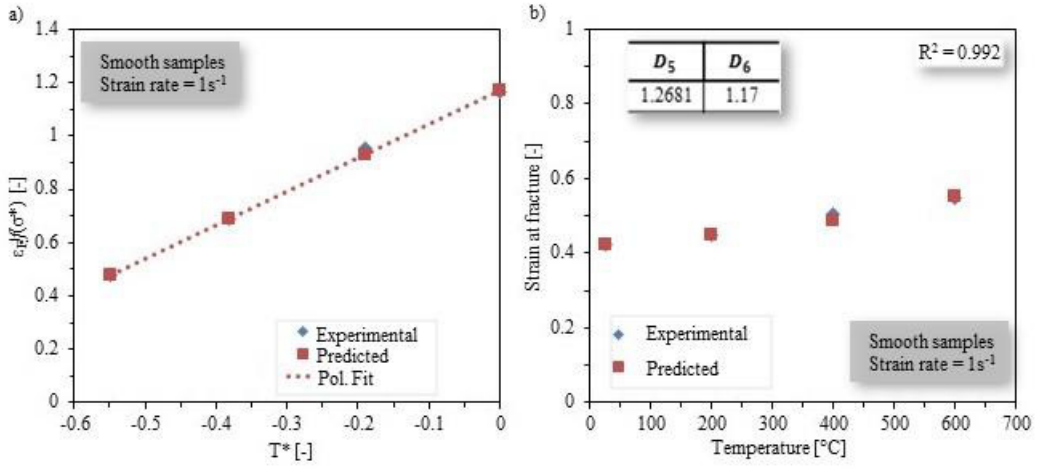

Figure 6: a) Strain at fracture-to-triaxiality factor ratio vs the homologous temperature and b) comparison between the experimental and predicted strains at fracture within Range A (25-600°C).

Within Range B, the relationship between the two members of Eq. (10) is not linear anymore, but it becomes a polynomial function (Figure 7a). On this basis, Eq. (10), representing the strain at fracture sensitivity to temperature in the Johnson-Cook fracture criterion, was modified according to Eq. (12):

$$\frac{\varepsilon_F}{[D_1+D_2\cdot e^{D_3\cdot\sigma^*}]} = D_I \cdot T^{*2} + D_{II} \cdot T^* + D_{III} \tag{12}$$

The values of the constants D_I, D_{II} and D_{III} were again identified through a non-linear regression analysis by minimizing the difference between the experimental and predicted data. The resulting constants, as well as the comparison between the experimental and the predicted values, calculated out through the new formulation representing the effect of temperature on the strain at fracture (Eq. (12)), are reported in Figure 7b, and, as it can be seen, the experimental and predicted values almost overlap.

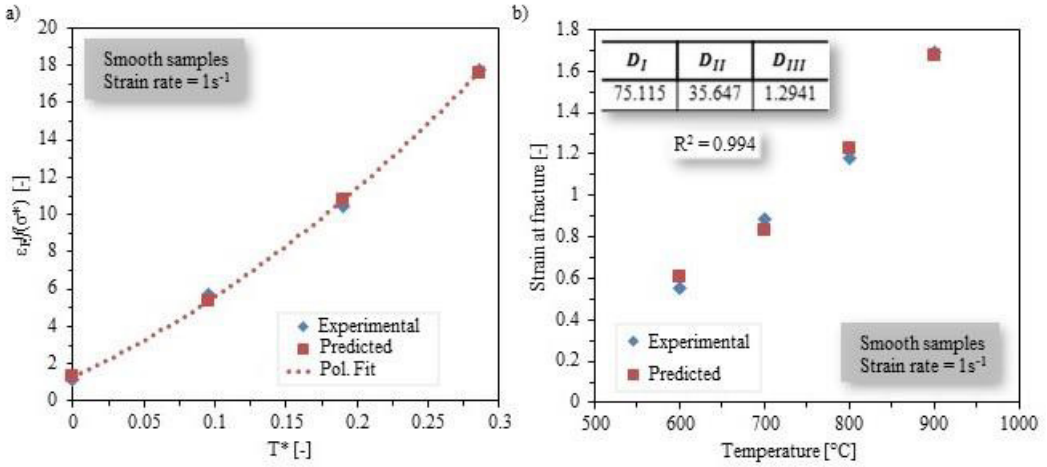

Figure 7: a) Strain at fracture-to-triaxiality factor ratio vs the homologous temperature and b) comparison between the experimental and predicted strains at fracture within Range B (600-900°C).

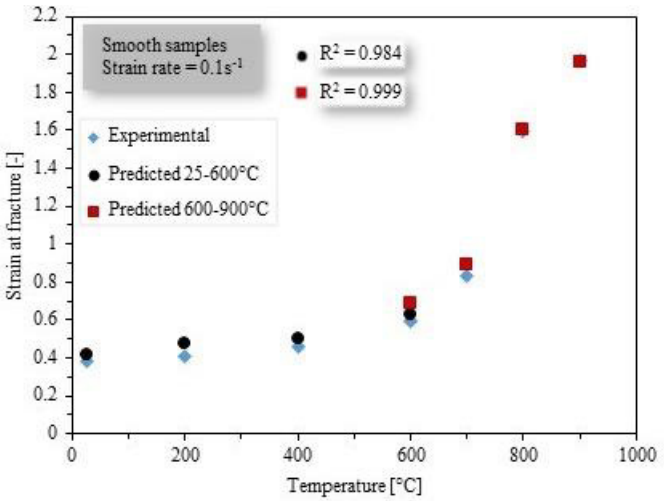

Figure 8: Comparison between the experimental and predicted strains at fracture in Range A (25-600°C) and Range B at 0.1 s^{-1}.

4.2 Validation of the modified Johnson-Cook fracture criterion

The predictability of the modified Johnson-Cook fracture criterion was verified on the basis of the seven tensile tests performed on smooth samples at all the testing temperatures, but at a strain rate ($\dot{\varepsilon} =$ 0.1 s^{-1}) lower than the reference one. The strains at fracture resulting from these tests were used to evaluate the accuracy of the model when applied to testing conditions different from the ones employed in the calibration procedure. Figure 8 shows the comparison between the experimental and the predicted strains at fracture in the two temperature ranges for the strain rate of 0.1 s^{-1}. As it can be seen, the modified criterion for range A, represented by Eq. (11), allows a good prediction, which is witnessed by the value of correlation coefficient reported in Figure 8. Within the high temperature range B (600-900°C), the modifications proposed in Eq. (12) assure a better accuracy, which is proved by the higher value of the correlation coefficient. It is worth to note that at 600°C, which is the temperature marking a change in the material ductility as a function of the temperature (Figure 2a), the criterion calibrated

for range A shows a greater accuracy in predicting the correspondent experimental strain at fracture than the one calibrated for range B.

5 Conclusions

The paper proposed a modified version of the Johnson-Cook fracture criterion to predict the ductile fracture occurrence in Ti6Al4V sheets deformed in a wide range of testing temperatures spanning from room temperature to 900°C. The modifications of the original criterion are based on the ductility characteristics that the Ti6Al4V presents at varying temperature. In particular, two different formulas of the criterion were proposed for the two considered temperature ranges, namely 25-600°C and 600-900°C. On the basis of the reported results, the following conclusions can be drawn:

- In the low temperature range A (25-600°C), the strain at fracture sensitivity to temperature is linear, as the original Johnson-Cook fracture criterion asserts;
- In the high temperature range B (600-900°C), a modified version of the original Johnson-Cook criterion is proposed since the relationship between the strain at fracture and the temperature becomes a polynomial function;
- The overlap between the experimental and predicted strains at fracture in the two ranges witnesses a good predictability of the models;
- The validation of the proposed criterion, performed by using the values of the strains at fracture resulted from tensile tests performed at 0.1 s^{-1} and not used for the criterion calibration, shows a good predictability for both the temperature ranges as the temperature is higher than 400°C. At lower temperatures, where the strain at fracture sensitivity to the strain rate is negligible, the criterion predictions are slightly different from the experimental data;
- At 600°C, the temperature which marks the change of the material ductility as a function of the temperature, the linear model obtained for range A provides a better prediction.

References

Algarni, M., Bai, Y. and Choi, Y., A study of Inconel 718 dependency on stress triaxiality and Lode angle in plastic deformation and ductile fracture. *Engineering Fracture Mechanics,* 2015, Vol. 147: pp. 140-157.

Børvik, T., Hopperstad, O., Berstad, T. and Langseth, M., A computational model of viscoplasticity and ductile damage for impact and penetration. *European Journal of Mechanics A/solids,* 2001, Vol. 20, p. 685–712.

Boyer, R., Welsch , G. and Collings, E., *Material properties handbook: titanium alloys.* s.l.: 1994, ASM International..

Bruschi, S., Altan, T., Banabic, D., Bariani, P.F., Brosius, A., Cao, J., Ghiotti, A., Khraisheh, M., Merklein, M. and Tekkaya, A.E., Testing and modelling of material behaviour and formability in sheet metal forming. *CIRP Annals - Manufacturing Technology,* 2014, Vol. 63/2: pp. 727-749.

Chen, F. and Chiu , K., Stamping formability of pure titanium sheets. *Journal of Material Precessing Technology,* 2005, Vol. 170: pp. 181-186.

Gordon, R. and Johnson, W., Fracture characteristics of three metals subjected to various strains, strain rates, temperatures and pressures. *Engineering Fracture Mechanics,* 1985, Vol. 21: pp. 31-48.

Guzmán, C. F., Tuninetti, V., Gilles, G. and Habraken, A., Assessment of damage and anisotropic plasticity models to predict Ti-6Al-4V behavior. *Key Engineering Materials,* 2015, Vol. 651-653: pp. 575-580.

He, A., Xie, G., Zhang, H. and Wang, X., A comparative study on Johnson-Cook, modified Johnson-Cook and Arrhenius-type constitutive models to predict the high temperature flow stress in 20CrMo alloy steel. *Materials and Design,* 2013, Vol. 52: pp. 677-685.

Li, H., Fu, M., Lu, J. and Yang, H.,. Ductile fracture: experiments and computations. *International Journal of Plasticity,* 2011, Vol. 27: pp. 147-180.

Ling-Yun, Q., Gang , F., Pan , Z. and Qian, W., Experimental and numerical investigations into the ductile fractureduring the forming of flat-rolled 5083-O aluminum alloy sheet. *Journal of Materials Processing Technology,* 2015, Vol. 220: p. 264–275.

Lin, L., Wang, H., Ni, M., Rui, Y., Cheng, T.Y., Cheng, T.K., Pan, X., Li, G. and Lin, C., Enhanced osteointegration of medical titanium implant with surface modifications in micro/nanoscale structures. *Journal of Orthopaedic Translation,* 2014, Vol.2: pp. 35-42.

Li, X., Guo, G., Xiao, J., Song, N. and Li, D., Constitutive modeling and the effects of strain rate and temperature on the formability of Ti-6Al-4V alloy sheet. *Materials and Design,* 2014, Vol. 55: pp. 325-334.

Majorell, A., Srivatsa , S. and Picu, R., Mechanical behavior of Ti-6Al-4V at high and moderate temperatures—part I: experimental results. *Materials Science and Engineering A,* 2002, Vol. 326: pp. 297-305.

Merklein, M., Maier, A., Kinnstatter, D., Jaremenko, C. and Affronti, E., A New Approach to the Evaluation of Forming Limits in Sheet Metal Forming. *Key Engineering Materials,* 2015, Vol. 639: pp. 333-338.

Odenberger, E., Schill , M. and Oldenburg , M., Thermo-mechanical sheet metal forming of aero engine components in Ti-6Al-4V—part 2: constitutive modelling and validation. *International Journal of Material Forming,* 2013, Vol. 6: pp. 403-416.

Tan, J.q., Zhan, M., Liu, S., Huang, T., Guo, J. and Yang, H., A modified Johnson–Cook model for tensile flow behaviors of 7050-T7451aluminum alloy at high strain rates. *Materials Science and Engineering A,* 2015, Vol. 631: pp. 214-219.

Valoppi, B., Bruschi, S. and Ghiotti, A.,. Mechanical and anisotropic characteristics of Ti6Al4V sheets deformed at elevated temperatures. In: *Proc. of the 7th Forming Technology Forum on warm and hot forming,* 2014, pp. 145-150. Enschede, the Netherlands.